Society of Petroleum Engineers

SPE-182608-MS

Simulation of Matrix-Fracture Interaction in Low-Permeability Fractured Unconventional Reservoirs

D. Y. Ding, N. Farah, and B. Bourbiaux, IFP Energies Nouvelles; Y-S. Wu, Colorado School of Mines; I. Mestiri, IFP Energies nouvelles

This paper was prepared for presentation at the SPE Reservoir Simulation Conference held in Montgomery, TX, USA, 20–22 February 2017.

Abstract

Unconventional reservoirs, such as shale-gas or tight-oil reservoirs, are generally highly fractured, including hydraulic fractures, stimulated and non-stimulated natural fractures of various sizes, embedded in low-permeability formations. One of the main production mechanisms in unconventional reservoirs is the flow exchange between matrix and fracture media. However, due to extremely-low matrix permeability, the matrix/fracture exchange is very slow and the transient flow may last several to tens of years, i.e. almost the entire production life. The commonly-used dual-porosity modelling approach involves a computation of pseudo-steady-state matrix-fracture transfers with homogenized fluid and flow properties within the matrix medium. This kind of model clearly fails to handle the long-lasting matrix/fracture interaction in very-low permeability reservoirs, especially for multi-pahse flow with phase change problems. Moreover, a dual-porosity model is not adapted for the simulation of matrix/fracture exchange when fractures are described by a DFN (Discrete Fracture Network). This paper presents an EDFM (Embedded Discrete Fracture Model) based on the MINC (Multiple INteracting Continua) proximity function to overcome this insufficiency of the conventional dual-porosity model.

Introduction

Unconventional tight-oil or shale-gas reservoirs require stimulation via hydraulic fracturing to create fracture networks for profitable exploitation. The injection of a high pressure fluid induces new channels or fractures in the rock and enhances the ultimate recovery. This operation also induces shear failure of the pre-existing natural fractures in shale formations, which results in natural fracture opening and propagation, and in the creation of an extensive, interconnected flowing network (Delorme et al. 2013). This complex multi-scale fracture network, including hydraulic and stimulated/non-stimulated natural fractures, together with the characteristics of extremely low permeability formation, results in a complex multi-medium reservoir and entails difficulties in the simulation of shale-gas or tight-oils production (see, for example, Mirzaei and Cipolla, 2012; Wu et al. 2014).

To model a realistic reservoir fracture network, discrete fracture models (DFMs) have received a great attention. These DFM models, that discretize explicitly all types of fractures, including hydraulic induced,

stimulated and non-stimulated natural fractures, are considered accurate for a conventional fractured reservoir modeling, but involve too many unknowns and often non-tractable numerical systems to solve. Moreover, the matrix-fracture interaction cannot be properly handled with this approach in very low permeability reservoirs.

To overcome the limitation related to high number of unknowns and CPU time, Lee *et al.* (2001) proposed a Hierarchical Fracture Model (HFM) to model fluid flow from natural fractured reservoirs by taking into account multi-length fractures. Their concept consists of discretizing explicitly long conductive fractures as major fluid conduits, while short and medium fractures are homogenized, leading to a higher effective matrix permeability. Based on this concept, various DFMs were tested and studied in the literature (see for example, Hajibeygi *et al.* 2011; Moinfar *et al.*, 2011, Norbeck *et al.*, 2014; Jiang et al.; 2014, Xu et al., 2016). These models rely on unstructured grids to conform the geometry and location of the fracture network, and they can significantly reduce CPU time for fluid flow simulation of naturally fractured reservoirs.

Karimi-Fard *et al.* (2004) and Matthai et al. (2005) developed DFMs based on an unstructured control-volume formulation, in which the rock matrix is modeled by 3D polyhedral cells and the fracture network is represented by a subset of the 2D interfaces separating grid cells. The physical domain is discretized using unstructured grids. However, these models cannot practically be used to simulate natural fractures, because of the associated prohibitive computational cost. Moreover, generation of such grid for an arbitrary fracture network can be a substantial challenge.

Moinfar *et al.* (2011 and 2013) introduced a new type of discrete fracture models called EDFMs (Embedded Discrete Fracture Models), which consists of modeling fractures embedded in a structured matrix grid. Norbeck *et al.* (2014) presents a variant model, where a numerical model was developed, aiming to capture the dynamic behavior of fractured reservoir systems, in which both the properties of individual fractures and the connectivity of fracture networks are expected to evolve over time.

In contrast with conventional reservoirs, unconventional shale-gas/tight-oil reservoirs are characterized by extremely-low matrix permeabilities. One of the main challenges in unconventional shale reservoir simulations is the flow transfer between matrix and fracture media. When matrix blocks have a large size, the traditional approach for simulating matrix-fracture transfers results in large errors in the prediction of field production. This is because it may take years to reach a pseudo-steady state flow regime in the matrix medium, due to the extremely low matrix permeability. A dual-porosity model, which computes an average pressure on a large matrix block, cannot describe the detailed pressure variation in the near-fracture zones.

To improve the accuracy for matrix-fracture interaction computation, using a MINC approach is a solution. MINC stands for "Multiple INteracting Continua", originally developed by Pruess and Narasimhan (1985) to model heat and multiphase fluid flow in fractured porous media. This concept is able to describe gradients of pressures, temperatures, or concentrations near matrix surface and inside the matrix by further subdividing individual matrix blocks into oneor multidimensional strings of nested meshes. Therefore, the MINC method treats interporosity flow in a fully transient manner by computing the gradients which drive interporosity flow at the matrix-fracture interface. As a result, the MINC model in general provides a better numerical approximation for fracture-matrix interactions than the double-porosity model. This method was applied to various studies of fractured reservoirs (see, for example, Wu and Pruess, 1988; Farhadinia and Delshad, 2010). It was also investigated by Ding *et al.* (2014) for the single-phase shale-gas simulations and by Farah *et al.* (2015) to study the fracturing fluid induced formation damage.

Recently, Jiang et al. (2014; 2016) applied the MINC approach to the EDFM. Based on the hierarchical approach, Jiang et al. (2014; 2016) homogenize short/low conductivity fractures, and use a MINC approach to simulate exchange between the matrix and the homogenized fracture media. Equivalent block sizes, which correspond to the effective fracture spacings in x, y and z directions, are determined on each simulation gridblock, and the matrix medium is then subdivided into nested volumes with the MINC to handle matrix-

fracture interaction. However, the detailed fracture network geometry is not taken into account in the MINC subdivision.

Farah and Ding (2016) proposed an EDFM based on the MINC proximity function (EDFM-MINC) to improve the modeling of matrix/fracture interaction. The MINC proximity function is computed according to the distance from all discrete fractures. So, the fracture geometry and location are taken into account via the proximity function, and all fractures, including high conductivity hydraulic fractures and homogenized stimulated/non-stimulated natural fractures, are considered in the matrix-fracture interaction. This approach is within the scope of a triple-porosity model, where the propped fractures, especially, hydraulic fractures, are explicitly discretized and other fractures are homogenized. In this paper, we present some improved techniques to ameliorate the transmissibility computation for the EDFM-MINC approach. In particular, an integral represented pressure distribution is used for the transmissibility calculation in the vicinity of hydraulic fractures. The connections between SRV (Stimulated Reservoir Volume) and non-SRV cells are also adapted to the presence of MINC subdivisions in SRV cells.

This EDFM based on the MINC proximity function is particularly useful for the simulation of multi-phase flow with phase change problems. For example, in a tight-oil reservoir, when the fracture pressure drops below the bubble point, gas starts to appear in the matrix formation near the fracture faces. The MINC method is suitable to simulate this kind of phenomena, which cannot be handled with a standard dual-porosity approach. Some numerical examples are presented to compare the EDFM-MINC approach, the dual-porosity model, and a fine-mesh single-porosity model with explicitly discretized fractures that is considered as the reference solution. Both tight-oil and shale-gas with phase change problems are investigated. The results show that the dual-porosity model is not suitable for the simulation of low-permeability unconventional reservoirs, and the proposed EDFM-MINC approach improves greatly the accuracy. Using the MINC based approach, a compromise between simulation accuracy and CPU time is found.

Mathematical model

We present, in the following, the governing equations for three-phase, multi-component flow with a dual-porosity approach. The mole conservation for each component *c* in a dual-porosity/dual-permeability system is expressed as:

$$\frac{\partial}{\partial t}\left[\emptyset^f \sum_p \left(\rho_p^f C_{cp}^f S_p^f\right)\right] + div\left[\sum_p \left(\rho_p^f C_{cp}^f \vec{u}_p^f + \vec{J}_{cp}^f\right)\right] - Q_{cp}^{mf} - \sum \rho_p^f C_{cp}^f q_p^f = 0 \quad (1)$$

and

$$\frac{\partial}{\partial t}\left[\emptyset^m \sum_p \left(\rho_p^m C_{cp}^m S_p^m + v_{sg}\right)\right] + div\left[\sum_p \left(\rho_p^m C_{cp}^m \vec{u}_p^m + \vec{J}_{cp}^m\right)\right] + Q_{cp}^{mf} - \sum \rho_p^m C_{cp}^m q_p^m = 0 \quad (2)$$

where the superscript *f* refers to the fracture and the superscript *m* to the matrix, the subscript *p (p = w, o, g)* refers to the phase water, oil or gas; $\emptyset^m$, $\emptyset^f$ are respectively the matrix and fracture porosity; C_{cp}^M (for medium $M = f$ *or* m) is the mole fraction of the component *c* in phase *p*; S_p^M ($M = f$ or m) is the saturation of the phase *p*; ρ_p^M is the mole density of phase *p;* v_{sg} corresponds to the gas sorption term, that appears only in the gas component conservation equation in the matrix medium; $\vec{u}_p^M$ is the velocity of phase *p* in medium *M*; $\vec{J}_{cp}^M$ is the molecular diffusion and dispersion flux of component *c* in phase *p* in medium *M*. Also, q_p^M is

the sink/source term of phase p per unit volume of formation in medium M; and Q_{cp}^{mf} is the matrix-fracture transfer rate of component c in phase p per unit bulk volume of reservoir.

The phase velocity is expressed with the Darcy's law in both the matrix and fracture media with

$$\vec{u}_p^M = -k_M \frac{k_{rp}^M}{\mu_p^M} \, grad(\Phi_p^M) \tag{3}$$

and

$$\Phi_p^M = P_p^M - \rho_p^M gZ \tag{4}$$

where $M = f$ or m represents the fracture or the matrix medium; Z is depth (positive, increasing downwards); g is the algebraic value of gravitational acceleration projection on Z axis; k is the absolute permeability; P_p the pressure of phase p, μ_p the viscosity of phase p; k_{rp} the relative permeability of phase p.

In a dual-porosity approach, the discrete fracture network is homogenized. In particular, we need the equivalent permeability and porosity in the homogenized fracture medium. The MINC method can be considered as a generalization of the dual-porosity approach. This method treats the inter-porosity flow inside the matrix media in a fully transient way for the matrix-fracture exchange.

For the single-porosity model, only the Eq.(2) is considered. The absolute permeability can be either the matrix permeability or fracture permeability according to the considered location or the simulation cell. To build a reference solution with the single-porosity model, very fine meshes are used for the discretization of the matrix medium, and the fractures are explicitly discretized through their intersect nodes. The flow exchange between a matrix cell and a fracture node is computed using the method described in Sarda et al. (2002).

In a reservoir study, it is difficult to use a finely meshed single-porosity model by discretizing explicitly all the fractures, due to the large number of grid cells and high CPU time. Using the EDFM-MINC approach is a solution. According to the EDFM concept, we discretize explicitly only high conductive hydraulic fractures, and all other fractures are homogenized. In the SRV, the EDFM-MINC is used to simulate, on one side the interaction between the homogenized fracture medium and the matrix medium using MINC proximity function, and on the other side the interaction between the homogenized fracture medium and the discrete hydraulic fractures.

Numerical method and simulation approach

The system of equations (Eqs. (1)-(4)) is discretized in space using a control-volume method, where time discretization is carried out using a backward, first order, finite difference scheme. The control-volume method is very flexible for handling the interactions between various kinds of continua. For example, the exchange between two grid cells is given by (Fig. 1):

$$F_{p,ij} = \lambda_{p,ij} T_{ij} (\Phi_{p,j} - \Phi_{p,i}) \tag{5}$$

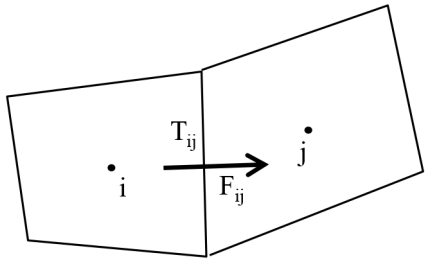

Figure 1—Flux approximation in the control-volume method

where T is the transmissibility between two grid cells i and j, $\lambda_{p,ij} = \frac{k_{rp}}{\mu_p}$ is the mobility term of phase p. The exchange between the matrix and fracture media for the dual-porosity model is computed with

$$Q_p^{mf} = \lambda_p^{mf} \sigma (\Phi_p^m - \Phi_p^f) \tag{6}$$

with σ the shape factor. If the block dimensions are known, the following shape factor is used for the 2D matrix-fracture exchange:

$$\sigma = \frac{10}{a^2} + \frac{10}{b^2} \tag{7}$$

where a and b are the block sizes in x and y directions respectively. Otherwise, the shape factor is computed with Eq.(12) given hereafter by considering a particular case in MINC with only one matrix subdivision. The accuracy of the discretized scheme depends greatly on the transmissibility and the shape factor formulation. This is particularly true in low-permeability unconventional reservoirs.

One of the key issues in numerical modeling for unconventional shale-gas or tight-oil reservoirs is the handling of fluid flow exchanges in the presence of a complex fracture network, including hydraulic and propped fractures (white curves) and stimulated/non-stimulated natural fractures (Fig. 2). All these fractures are connected to each other, leading to a very complex DFN. The EDFM approach takes into consideration three media: (a) discrete high-conductivity hydraulic fractures, (b) homogenized fracture medium for the stimulated/non-stimulated natural fractures, and (c) matrix medium. In the SRV, all three media are considered. Outside the SRV, only a single-porosity approach is used. For an EDFM, the flow exchange term can always be written in the form of Eq.(5) or Eq.(6), but the transmissibility T depends on the fracture geometry and on the permeability of the interacting medium in the cells under consideration.

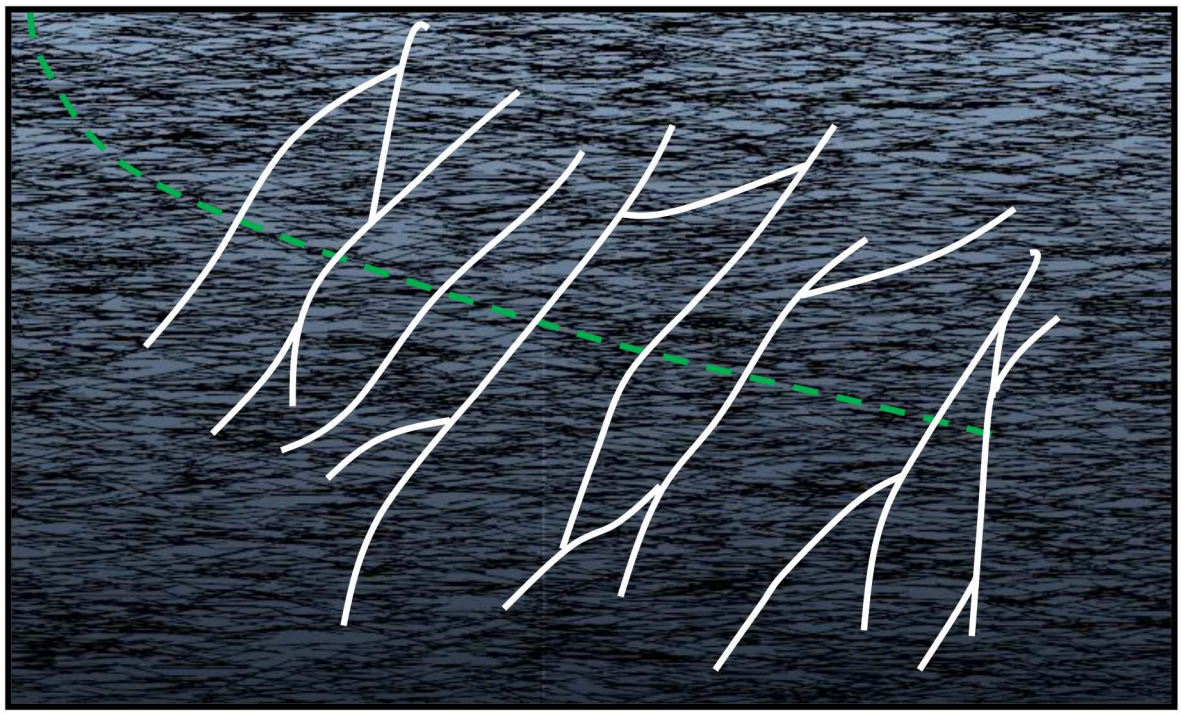

Figure 2—Illustration of the hierarchical model with multi-scale fractures: high conductivity hydraulic fractures (white lines) and low conductivity induced and natural fractures (black lines)

In this paper, we classify the fractures, generated by a geostatistical model, based on conductivity criteria. Hydraulic fractures and propped stimulated fractures are usually highly conductive, and will be explicitly discretized due to their very important role in the production. Other fractures are homogenized. It must be mentioned that among all interactions, the modeling of flow exchange between matrix and fracture is extremely important because of the ultra-low matrix permeability. On the other hand, it is assumed that no flow occurs between two matrix cells in the SRV.

Flow within the discrete network of hydraulic fractures

Highly conductive fractures, such as hydraulic fractures, have more dominating influence on fluid flow than short and medium fractures. These highly conductive fractures are explicitly discretized and modeled using fracture nodes. Each intersection of two (or more) high conductivity fractures (black lines in Fig. 3) constitutes a fracture node (red node in Fig. 3). A fracture volume and an exchange surface area are assigned to each fracture node to compute fluid flow inside the high conductivity fractures (see, for example, Khvoenkova and Delorme 2011).

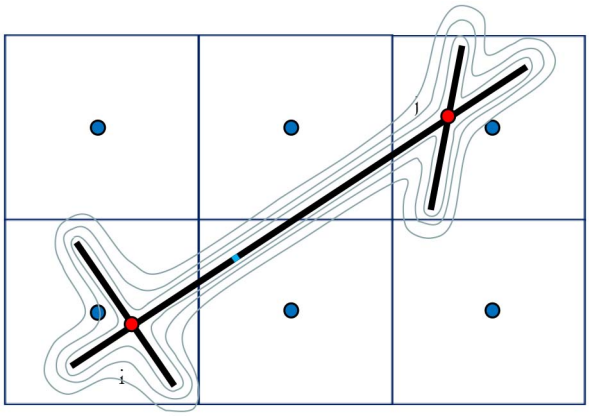

Figure 3—Pressure distribution (iso-pressure lines) around fractures

Exchange between high-conductivity fractures and the homogenized fracture medium

Most DFMs, including EDFMs, assume a linear pressure distribution around fractures (see, for example, Lee et al., 2001; Moinfar et al., 2011; Farah et al. 2016), and they use a linear approximation to compute flow exchange between a discrete fracture and a continuous medium. Under this assumption, the transmissibility T_{kj} between a homogenized fracture cell k and a hydraulic fracture node j is given by:

$$T_{kj}^{fF} = k_{fk} \frac{A_{kj}}{< d_{kj} >} \tag{8}$$

where k_{fk} is the equivalent permeability of the cell k, A_{kj} is the exchange surface area between the hydraulic fracture attached to node j and cell k, $< d_{kj} >$ is the average distance between cell k and the hydraulic fracture associated with node j.

However, the assumption of linear pressure distribution is not always true, especially, near the fracture extremities and the fracture intersection zones (Fig. 3). The iso-pressure lines are affected by the presence of other fractures and the extremity effects.

To get a more realistic pressure distribution around fractures, Ding et al. (2014) proposed to use an integral method to represent iso-pressure distribution in the near-fracture field for a steady-state flow. The integral representation gives a suitable description for both the linear iso-pressure line near the middle of an isolated fracture and curved iso-pressure lines near the fracture ends or intersections. Once the pressure

field around the hydraulic fracture is known, the transmissibility between the homogenized fracture cell k and the hydraulic fracture node j can be identified by the Darcy's law with the following formula:

$$T_{kj}^{fF} = \left| \frac{Q_{kj}}{P_{f,k} - P_{F,j}} \right| \tag{9}$$

where, $P_{F,j}$ is the pressure on the node j, $P_{f,k}$ is the average pressure on the homogenized fracture cell k, Q_{kj} is the flow rate from the cell k to the fracture node j through the exchange surface A_{kj}. All these variables are computed using the integral method (Ding *et al*. 2014).

Flow within the homogenized fracture medium

In general, the transmissibility between two homogenized fracture cells is calculated as follows:

$$T_{ij}^{f} = A_{ij} \frac{k_{fi} k_{fj}}{d_i k_{fj} + d_j k_{ij}} \tag{10}$$

where A_{ij} is the exchange surface between the two homogenized cells i and j, k_{fi} and k_{fj} are the homogenized fracture permeabilities on the cells i and j, d_i and d_j are the distance from the cell center to the exchange surface (Fig. 4). However, the above equation is not suitable for flow simulation near high conductive hydraulic fractures. Let us consider a hydraulic fracture that intersects one of two neighbouring homogenized fracture cells (the red line in Fig. 4). If we use Eq.(10) for the transmissibility calculation, the fluid in Cell i will be driven first to the center of Cell j and then back to the hydraulic fracture. This approach underestimates the flow rate between Cell i and the hydraulic fracture, if they are quite close, as shown in Fig. 4.

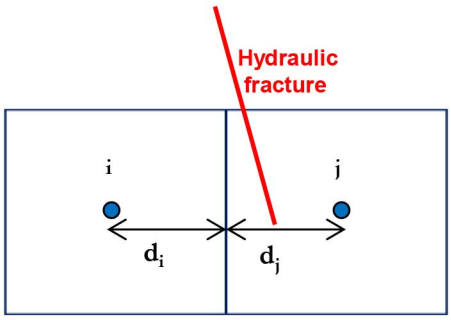

Figure 4—Transmissibility betweentwo homogenized fracture cells

To take into account the impact of the presence of hydraulic fractures on the fluid flow in the homogenized medium, we propose to use again the integral representation for transmissibility computation. If one of the homogenized cells intersects with a conductive fracture, it is not convenient to represent the pressure of this cell at its cell center. Instead, the average cell pressure can be represented using an integral formula (Ding et al., 2014). In this case, we propose to determine the transmissibility between these two cells through an identification from the Darcy's flow by:

$$T_{ij}^{f} = \left| \frac{F_{i,j}}{P_{f,i} - P_{f,j}} \right| \tag{11}$$

where $P_{f,i}$ and $P_{f,j}$ are the average fracture pressures of cells i and j, given by the integral formulas; and F_{ij} is the flow exchange between these two cells, also calculated from the integral formula, which corresponds to the pressure normal directive on the interface between the two cells.

If both considered homogenized cells do not intersect any discretized conductive fracture, we use the pressures defined at the center of the grid cells and the transmissibility is determined with the linear approach Eq. (10).

These two different transmissibility computation methods, linear approach with Eqs.(8) and (10) and integral based approach with Eqs.(9) and (11), will be compared through an example hereafter.

Exchange between matrix medium and fractures

One of the key issues in the modeling of low-permeability fractured reservoir is the matrix-fracture interaction. To improve the accuracy, the MINC concept is applied. The MINC method can be considered as a generalization of the dual-porosity (DP) concept. The main difference between MINC method and a DP model is in the matrix-fracture exchange known also by "inter-porosity flow". The DP method simulates matrix-fracture exchange on the basis of a pseudo-steady state flow, while MINC method treats the problem entirely by numerical approach in a fully transient way. In general, the MINC model provides a better numerical approximation for transient fracture-matrix interactions than a dual-porosity model.

The basic idea of the MINC is to subdivide a matrix cell according to the distance from the fractures. Although using iso-pressure line for cell subdivisions might be more accurate for inter-porosity flow simulation (Ding et al. 2014; Cai et al. 2015), for the reason of simplicity, a generalization of this kind of approaches to the EDFM is not discussed in this work. The choice of MINC sub-cell thicknesses is not discussed herein, although it can be optimized in order to best follow the local evolution of pressure in matrix medium, as shown by Famy et al. (2005) for a two-phase flow transfer problem.

In the EDFM, a matrix cell may interact with all sorts of fractures, including both high conductive hydraulic fractures and low-conductivity stimulated/non-stimulated natural fractures. All these interactions are modeled using the MINC approach. So, when we sub-divide a matrix cell, the sub-cells are constructed by considering the distance to both hydraulic and connected natural fractures as shown in Fig. 5. As hydraulic fracture nodes are not necessarily inside the considered matrix cell, for simplicity, we affect first all flow exchanges between matrix and fractures to the homogenized fracture cell, and then the homogenized cells exchange with hydraulic fracture nodes. In other words, the modeling of matrix-fracture interaction takes into account all types of connected fractures, but the exchange between a matrix cell and hydraulic fractures is performed via a homogenized fracture cell in the numerical modeling. It has to be mentioned that the equivalent permeabilities and porosities are determined with only the low conductivity fractures, while the exchange between matrices and fractures involve all sorts of fractures.

To subdivide a matrix cell, a number of points are randomly launched inside the cell. The distance between a random point within the matrix and all connected fractures inside the cell is calculated. Thus, the histogram of random point distances to the fractures can be plotted. For example, Fig. 6a shows a histogram where distances are grouped by intervals of 0.25 ft for 1000 points launched in a square cell. Figure 6b is the cumulative distribution function of these 1000 points (denoted ς) with respect to the distance from the fractures.

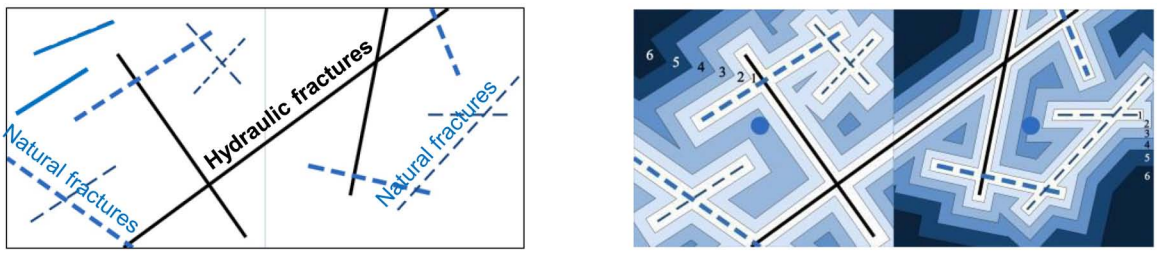

5a) a discrete fracture network (connected and isolated)

5b) computing the MINC proximity function for a MINC6 model

Figure 5—Illustration of the MINC method

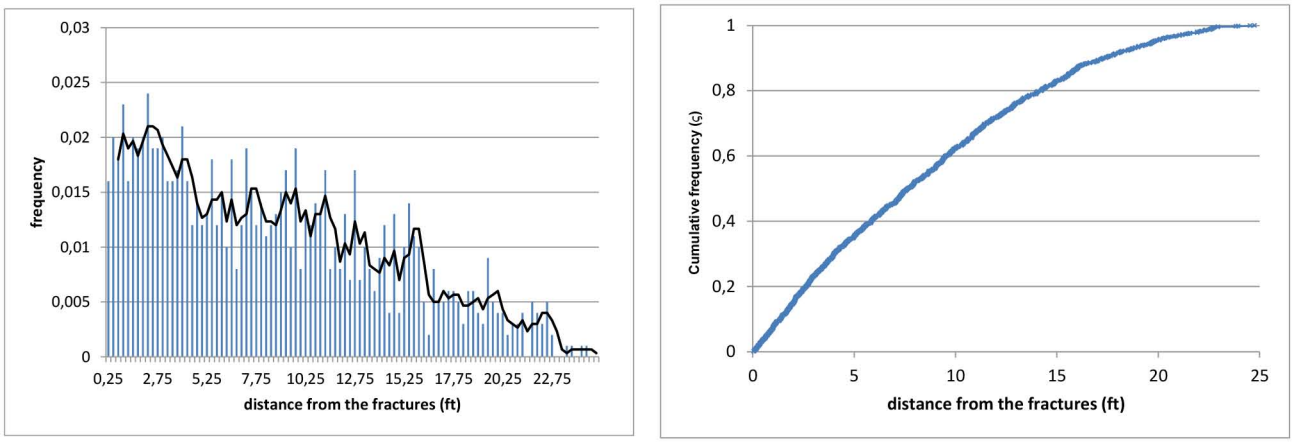

6a) histogram

6b) cumulative distribution function

Figure 6—Illustration of an example representing the point distribution versus the distance from the fractures

Using the distribution function, we can subdivide a matrix cell according to the distance from the fractures. Let $d_0 = 0 < d_1 < d_2 < \ldots < d_n = d_{max}$ be a discretization on the interval $[0, d_{max}]$ with d_{max} the maximum distance from the cell to the fractures, the i^{th} MINC sub-block is constructed by the volume of matrix cell with a distance to the fractures comprised between d_{i-1} and d_i. The first MINC sub-block connects to the homogenized fracture medium, and the transmissibility T_j^{fm} between this first MINC subdivision and a fracture cell j is given by:

$$T_j^{fm} = 2\frac{k_{mj}}{d_1} A_j^{fm} \tag{12}$$

where A_j^{fm} is the area of the fracture surface in the cell j, k_{mj} is the matrix permeability of the cell j. The transmissibility between two sub-cells i and $i+1$ is given by:

$$T_i^m = \frac{A_i K_m}{d_{i+1} - d_i} \tag{13}$$

where A_i is the area of the interface between these two sub-cells. This area corresponds, in fact, to the derivative of the cumulative volume of matrix with respect to the distance from the fractures. The cumulative volume of matrix within a given distance from the fractures in the cell is obtained as the product of the cumulative random-points fraction ς (Fig. 6b) by the total bulk volume of the matrix cell. Therefore, the exchange area between two MINC matrix subdivisions i and $i+1$ can be approximated using a finite-difference approach as follows :

$$A_i = \frac{V_{i+1} - V_i}{d_{i+1} - d_i} = \frac{d\varsigma}{dx} V_{cell} \tag{14}$$

where V_i is the cumulative volume of matrix within a distance x from the fractures equal to d_i, and V_{cell} the cell volume.

Exchange between SRV and non-SRV

The contribution from the zone outside SRV is not negligible, especially for non-SRV cells very close to the SRV. Therefore, it is necessary to model correctly the fluid flow exchanges between SRV and non-SRV zones.

Figure 7 shows the connection between a SRV cell i and a non-SRV cell *j*. The cell i is subdivided by the MINC proximity function according to the distances from the fractures of that cell. So, the connections of cell *i* with the neighbouring cell *j* are computed via the MINC sub-cells of cell *i* that are found at the interface between the two cells. The transmissibility between the k^{th} MINC subdivision of Cell *i* and the non-SRV cell *j* is calculated as:

$$T_{ij}^{k} = \frac{k_{mi}k_{mj}}{d_j k_{mi} + d_i^k k_{mj}} A_{ij}^{k} \tag{15}$$

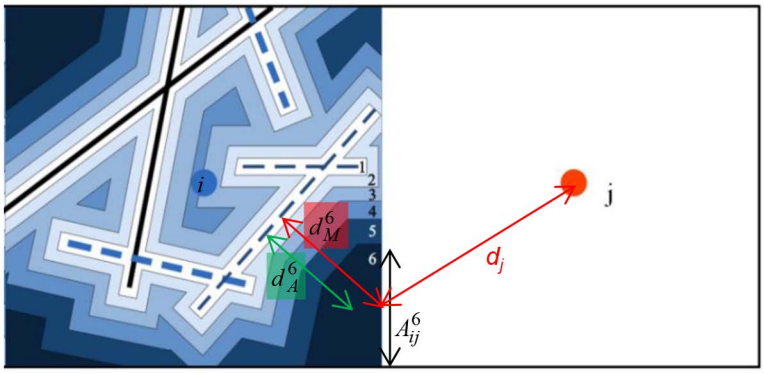

Figure 7—Connection between SRV and non-SRV cell

where, k_{mi} and k_{mj} and matrix permeabilities of cells *i* and *j*, respectively; A_{ij}^k is the exchange area between the cell *j* and the k^{th} MINC subdivision of cell *i*; d_j is the distance from the center of cell *j* to the exchange surface. d_i^k corresponds to the difference between the average distance d_A^k from the #*k* exchange area A_{ij}^k to the fractures and the average distance d_M^k of the MINC subdivision #*k* towards the fractures:

$$d_i^k = max(d_A^k - d_M^k,\ 0) \tag{16}$$

Note that we use only a positive distance, that is, if $d_i^k < 0$ then we define $d_i^k = 0$.

Numerical example

In all the examples, the reference solution is obtained on a very fine mesh with a single-porosity approach in which all fractures are explicitly discretized.

In the first example, we validate our EDFM based on the MINC proximity function with a Warren and Root's fracture network for a single-phase gas flow. Then, we study phase change problems for both tight-oil and shale-gas-condensate problems. For the tight-oil case, a Black-Oil model is used. Mobile water is assumed to be present in this reservoir. So, it is a three-phase flow problem. One of the issues for tight-oil simulation is the matrix/fracture interaction with phase change near the fracture faces. For the retrograde shale-gas case, a compositional model is used. The simulation cases presented hereafter are focused on the predictive capacity of the MINC method for modelling matrix/fracture interaction.

Single-phase flow on a regular fracture network

Shale-gas single-phase flow is considered on a Warren and Root's type fracture network to compare the EDFM-MINC and the dual-porosity model to the reference solution, which is obtained using a single-porosity model with very fine grid cells and explicit fracture discretization. The two types of transmissibility connections, based on the linear pressure and the integral represented pressure distributions, are compared.

Considering a stimulated reservoir volume of 1050×1000×300 ft as shown in Fig. 8. Apart from the highly-conductive hydraulic fractures, all other fractures are homogenized in the SRV and the MINC method is applied to subdivide the matrix medium based on the distance from the fractures. The hydraulic fracture length is 300 ft (red solid line in Fig. 8), and the spacing of the natural fracture network is 50 ft in both *x* and *y* directions. Table 1 summarizes the reservoir properties. A horizontal well is intersected at the middle of the hydraulic fracture (green point in Fig. 8), and it is assumed that the well production comes only through the hydraulic fracture.

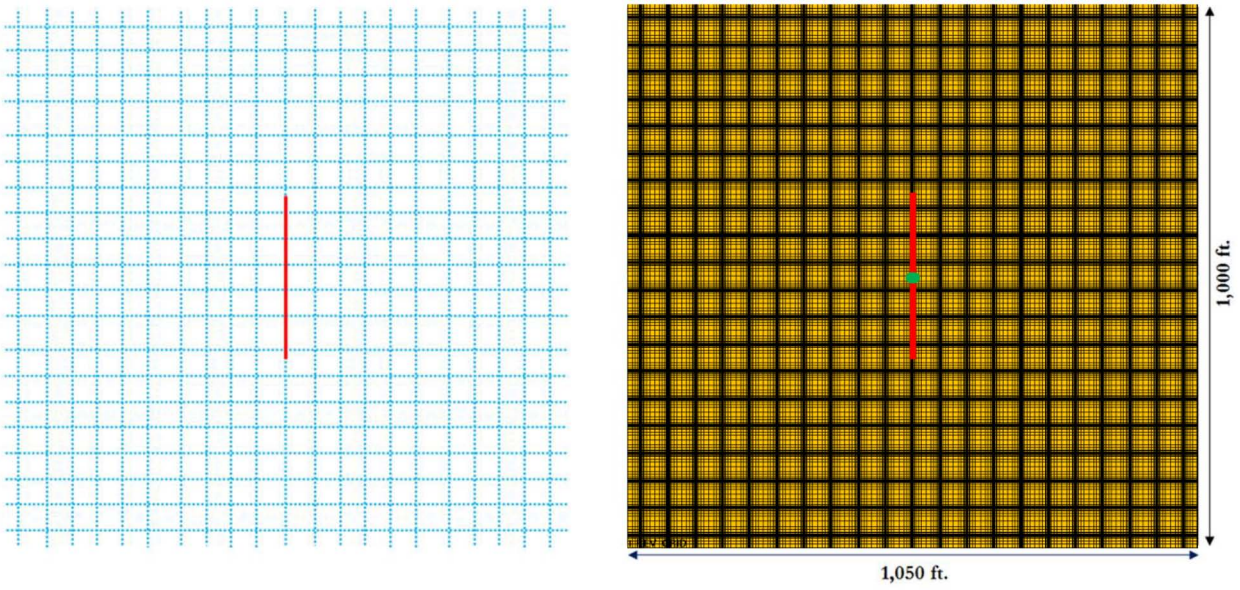

8a) a regular Warren and Root type fracture network

8b) explicit discretization of the fractures for the reference solution

Figure 8—Illustration of the regular fracture distribution

Table 1—Reservoir properties for the regular fracture network simulation

Property/Parameter	Value	Unit
Matrix permeability	0.0001	mD
Hydraulic fracture permeability	50	D
Induced fracture permeability	200	mD
Fracture width	0.01	ft
Induced fracture width	0.001	ft
Reservoir net thickness	300	ft
Initial reservoir pressure	3800	psi
Bottom hole well pressure	1000	psi

As the fractures are regularly distributed and oriented to the grid axe directions, we can accurately compute the equivalent permeabilities on the homogenized fracture medium. A MINC6 subdivision, which means that each matrix cell is subdivided by 6 sub-volumes, is used for the EDFM-MINC approach. Fig. 9 presents the cumulative gas production simulated with the EDFM-MINC, the dual-porosity model and the single-porosity model during 16000 days. For the EDFM-MINC model, two transmissibility formulas (linear based and integral based approaches) are compared. Obviously, the EDFM-MINC model provides a much better result than the dual-porosity model, and the integral based transmissibility approach is more accurate than the linear based transmissibility formula. The dual-porosity model greatly underestimates the

gas production and is not suitable for fractured low-permeability reservoir simulations. Our EDFM-MINC shows the ability of predicting gas production from unconventional fractured gas reservoirs, while a dual-porosity model is inaccurate for such problems.

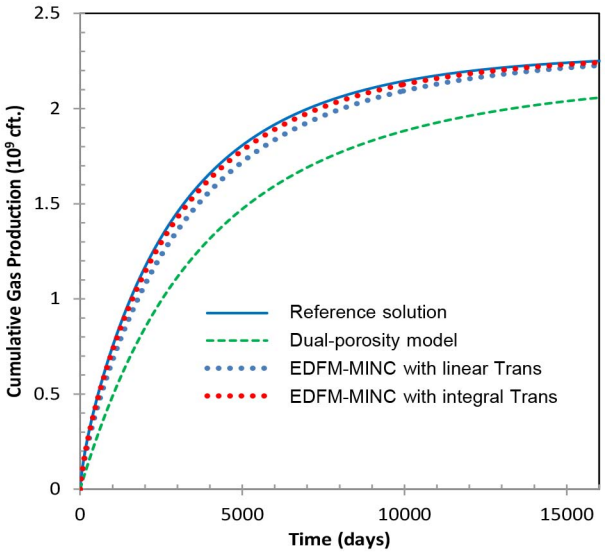

Figure 9—Comparison of simulations on the regular fracture network

Now, let us consider the case where the stimulated reservoir volume is not uniformly distributed in the whole simulation domain (Fig. 10). Figure 11 compares the cumulative gas production for the EDFM-MINC models with the two different transmissibility formulas and the reference solution (single-porosity model). Although all models give satisfactory results, using the transmissibility based on the integral pressure distribution is more accurate than the one based on a linear pressure distribution. Our EDFM-MINC method is also suitable for simulations containing non-SRV zones.

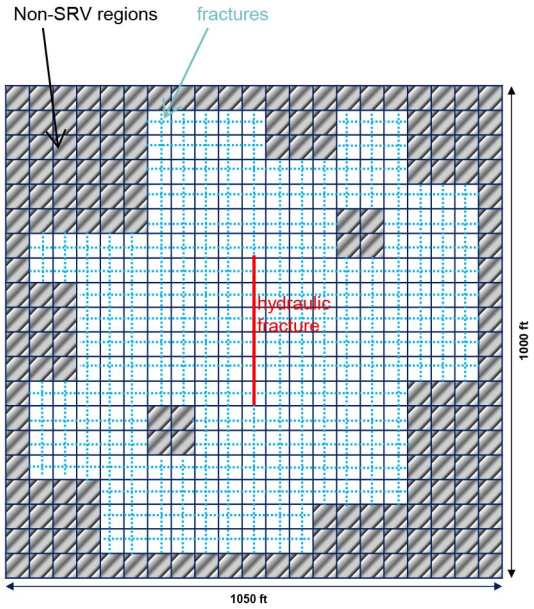

Figure 10—Warren & Root's fracture distribution with non-SRV regions

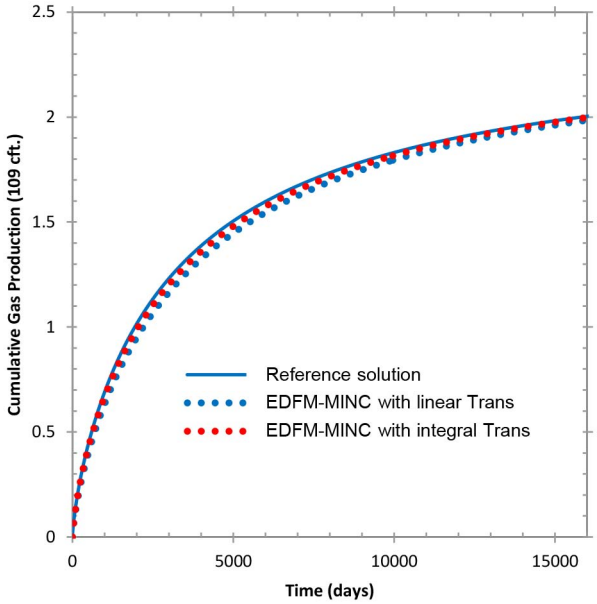

Figure 11—Simulations with non-SRV regions

Simulation of phase change in a single matrix block

In this session, we study the matrix-fracture exchange for multi-phase flow with phase change in a single matrix block. Consider a matrix block with an equal size of 100 ft in x and y directions, surrounded by fractures as shown in Fig. 12. The permeabilities are 2D and 0.001 mD respectively in the fracture and the matrix. The fracture width is 0.04 inch. The matrix porosity is 0.05. We consider a tight-oil case first and then a gas condensate case.

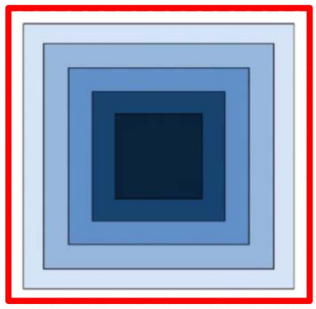

Figure 12—Simulation on a single matrix block with MINC subdivisions

To get the reference solution, a fine grid simulation is performed with 217 x 217 grid cells in the xy plane. The maximum cell size is 0.5 ft. The fracture is explicitly discretized with cells of size of 0.04 inch. The near fracture matrix cells are also very small, starting from size of 0.04 inch, and increased logarithmically with 12 gridblocks until the maximum size of 0.5 ft. This fine grid simulation is considered as the reference solution. For the dual-porosity simulation, only one matrix cell and one fracture cell are used, and the well is connected to the fracture cell. For the MINC approach, the matrix cell is subdivided according to the distances from the fractures (Fig. 12).

Tight-oil simulation

For the tight-oil case, a Black-oil model is used. The initial reservoir pressure is at 2900 psi, and the bubble point pressure is at 2710 psi. The bottom hole well pressure is imposed to 1160 psi. The matrix block also contains mobile water with a saturation of 0.39, while the irreducible water saturation is 0.1. As the fractures

have small volume, high permeability and with linear relative permeabilities (X-curves), the well production on the medium to long term results should correspond to the matrix-fracture exchange.

Different MINC subdivisions (MINC6, MINC8, MINC12, and MINC16) are applied. The simulation results are compared with the fine grid simulation on one side, and the dual-porosity model on the other side. Figure 13 presents the cumulative oil and gas productions. All MINC simulations give satisfactory results, while the dual-porosity approach is not accurate, especially for the gas production. This can be explained by the phase change near the fracture face. Figure 14 presents the GOR, which is a very sensitive data. In this example, the solution gas oil ratio is 960 cft/bbl. For the dual-porosity model, as only one matrix grid cell is used, the cell pressure remains above the bubble point pressure at early times. So the GOR of the dual-porosity model in the beginning is very close to the solution GOR. For the fine-grid reference simulation or the MINC method, the grid cells near the fracture are small, and the pressures on these cells drop very quickly below the bubble point pressure. This leads to higher GOR production at very early times. This high GOR corresponds to some field observations (Khvoenkova et al. 2015). Refining the MINC model (MINC8, MINC12 or MINC16) improves results if compared to the simulation of a coarse MINC model such as MINC6. After 400 days, GOR simulated with MINC models starts to diverge from the reference solution. This is because the oil production is very low (below 1 cft/day), and a small difference in oil production may lead to a strong GOR variation. Hence, comparison of long-term GOR in this example is not meaningful. Although all MINC subdivisions give globally satisfactory results, increasing the number of matrix subdivisions does not always ameliorate again the accuracy. In fact, with complex physics, such as a multi-phase flow with phase change, the simulation results, especially, GOR, are sensible to the grid sizes near the fractures. Nevertheless, we noticed that the general trends are good.

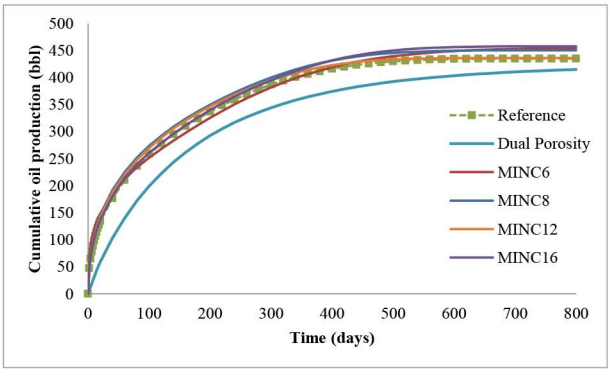

13a). Oil production

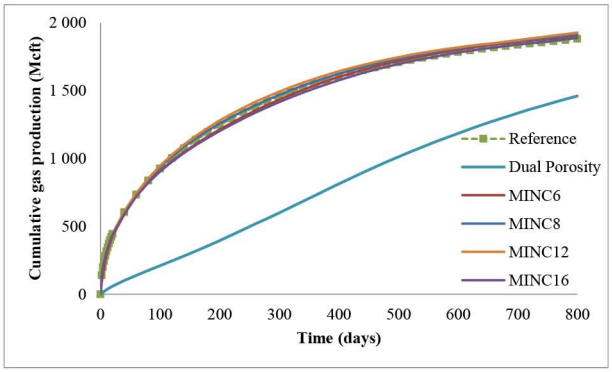

13b). Gas production

Figure 13—Cumulative oil and gas production in the single matrix block simulation in the tight-oil case

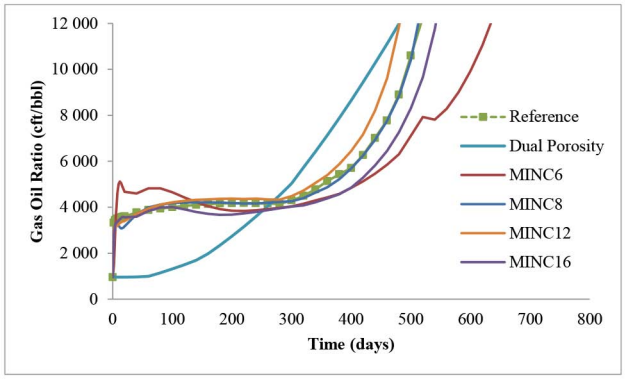

Figure 14—GOR in the single block simulation in the tight-oilcase

Figure 15 shows the pressure and gas saturation versus the distance to the fractures simulated with previous models. The MINC method predicts profiles that are very close to the ones given by the fine-grid model. Therefore, the MINC model can simulate the high production GOR from the fine-grid model, as the MINC pressure near the fracture is correctely computed. Figure 16 compares cumulative water productions. Again, the MINC approach gives reasonably accurate results, whereas the dual-porosity model prediction is not suitable.

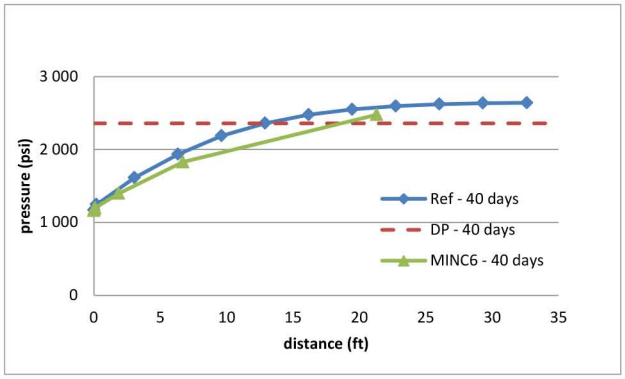

15a). Gas pressure

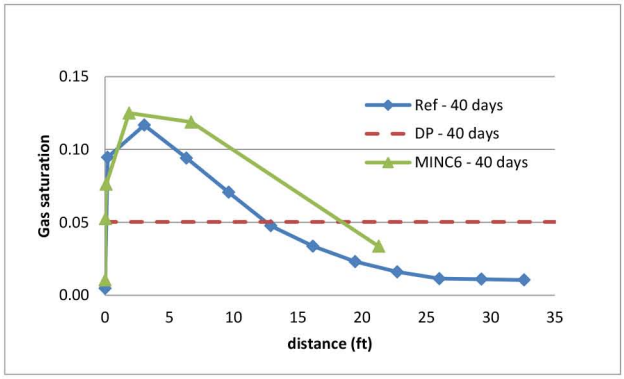

15b). Gas saturation

Figure 15—Gaspressure and saturation versus the distance fromthe fracture at 40 days

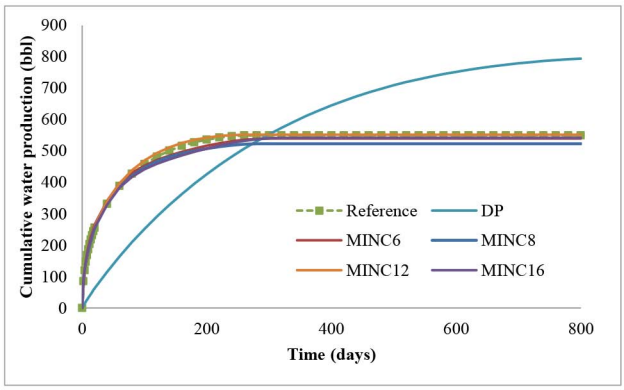

Figure 16—Cumulative water production in the single block tight-oil simulation

Now, we consider another test with a higher initial matrix pressure of 3480 psi and a higher bottom-hole well pressure of 2030 psi. Figure 17 presents the oil and gas productions, and Fig. 18 shows the produced GOR. Again, the MINC approach gives quite satisfactory results. In this test, the difference between the dual-porosity simulation and the reference solution is smaller, because the initial pressure is much higher than the bubble point pressure and for most of the time, the well effluent is an oil single-phase or includes a very small amount of liberated gas. As only a small volume of gas is present in the near-fracture zone, the GOR curves predicted by the fine-grid model or the MINC method are not as high as in the previous case.

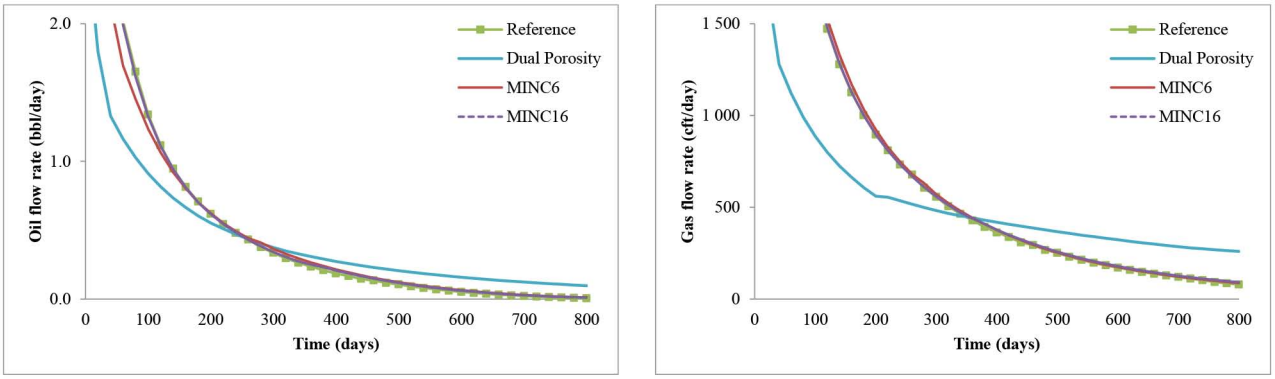

17a). Oil rate

17b). Gas rate

Figure 17—Oiland gasproduction witha higherinitial pressure

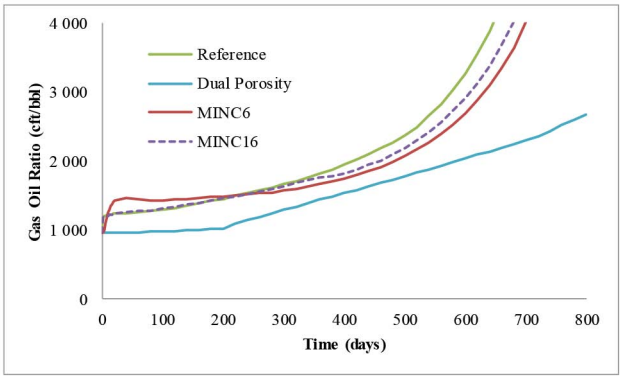

Figure 18—GOR in the single matrix block simulation with a higher initial pressure

Retrograde shale-gas simulation

For this gas condensate case, a compositional simulator is used. Eight components are presented in Table 2. This case is for a liquid-rich gas-condensate reservoir. In this test, the initial pressure is 6000 psi and the well flowing pressure (fracture pressure) is 1200 psi. The dew point pressure is around 3000 psi. The main flow feature of gas-condensate systems is the dropout of a liquid hydrocarbon phase within the pores of the reservoir rock as pressure falls below the dew point pressure. A condensate ring then builds up around the wellbore, where the pressure gradient is the highest, leading to a gas productivity decline.

Table 2—Gas composition

Component	Pc (psi)	Tc (F°)	Acentric factor	Molecular weight	Mole fraction (%)
CO2	1071.33	88.76	0.225	44.01	1.21
C1	667.78	-116.62	0.013	16.043	65.99
C2	708.34	90.07	0.0986	30.07	8.69
C3	618.70	205.94	0.1524	44.097	5.91
C4-C6	514.93	346.84	0.2158	66.869	9.67
Pseudol	410.75	378.41	0.3123	107.779	4.745
Pseudo2	247.56	598.34	0.5567	198.562	1.515
Pseudo3	160.42	832.19	0.9169	335.198	0.33

As depletion goes on, the condensate dropout takes place throughout the reservoir. The low mobility of condensate compared to that of gas, plus a possible capillary trapping, leads to an increase in the production gas-oil (gas-condensate) ratio, i.e., decrease of the condensate-gas ratio (CGR). That is, gas-condensate fluid systems encounter two main issues that are gas productivity drop and a poor recovery of condensate. For fractured reservoirs, the management of these production issues requires an accurate prediction of condensate dropout within the matrix blocks, which are actually the main source of recovered fluids. For the studied case, a single set of conventional (immiscible) relative permeability curves was considered, although the low interfacial tension conditions that sometimes prevail in the vicinity of the dew point pressure may impact these curves.

Figure 19 shows the gas and condensate production for the reference solution, the dual-porosity model and the MINC methods with 6 and 16 subdivisions. As in the tight-oil case, the dual-porosity model highly underestimates the gas production in early time. Figure 20 presents the pressure versus the distance from the fractures at different times (2 days, 20 days and 200 days) for the reference solution and the dual-porosity model. Clearly, the matrix pressure in the dual-porosity model, that is, the average pressure of the matrix block, remains above the dew point pressure (around 3200 psi) for a very long time, while the pressure near the fracture face drops very quickly with other models. So, the dual-porosity model produces much more condensate as no liquid drops out within the matrix block for more than two years. Figure 21 presents the condensate-gas ratio (CGR). For the dual-porosity model, CGR remains equal to the initial CGR of the single-phase fluid and starts to decrease only after 800 days, that is the time at which the slowly-decreasing average matrix block pressure reaches the dew point pressure. On the contrary, the reference model and the MINC-based models predict a very early drop in condensate production and CGR because of the matrix sub-gridding that allows condensation to rapidly take place near the fracture as the consequence of pressure dropping immediately to the fracture pressure there.

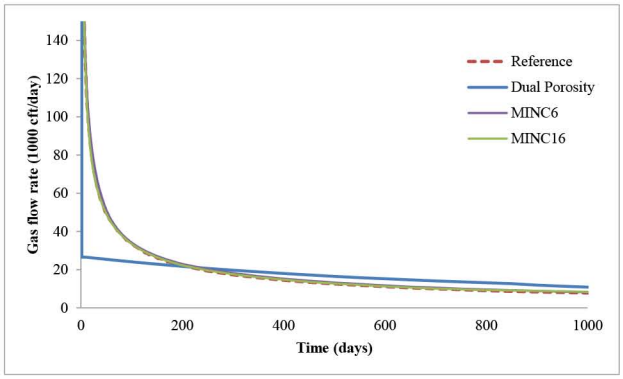

19a). Gas production

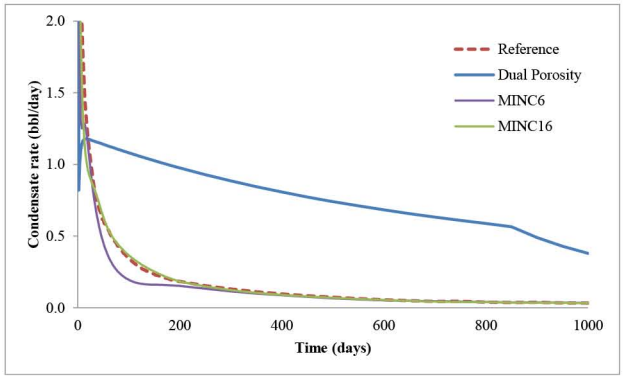

19b). Condensate production

Figure 19—Gas and condensate production in the single block simulation in the shale-gas case

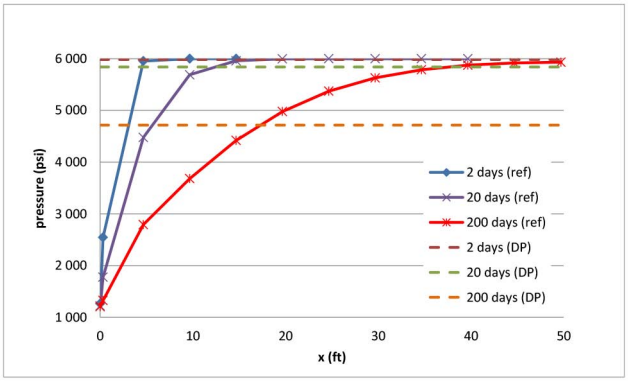

Figure 20—Pressure variation as a function of distance from the fracture in the single block simulation

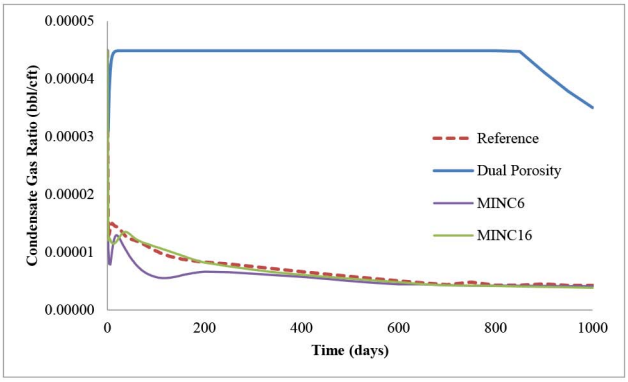

Figure 21—Condensate-gas ratio in the single-block simulation

These simulation results show that the MINC method gives very satisfactory results for multi-phase flow simulations in fractured reservoirs thanks to an accurate prediction of phase change impact on matrix-fracture transfers and reservoir production. This is a major limitation of dual-porosity models for their application to shale reservoirs.

A 2D synthetic case

Now, we consider a more realistic synthetic case, that is, a stimulated fracture network around a hydraulic fracture within a single reservoir layer, as shown in Fig. 22. We limit our simulations to a bounding box (or Stimulated Reservoir Volume) of 820 ft x 1800 ft x 20 ft. This reservoir contains two sets of natural fractures. One set of natural fractures is oriented with an average angle of 75° from the North to the North-East and has a mean length of 200 ft. The second set of fractures has an average orientation of 150° from the North to the South-East with a mean length of 400 ft. A hydraulic fracture oriented to the north is considered in the middle of this SRV with a length of 1480 ft, a width of 0.012 ft and a permeability of 20 D. These two sets of natural fractures are stimulated by hydraulic fracturing and have a thickness varying from 0.004 ft to 0.005 ft and permeability from 300 to 400 mD. In this example, we assume that natural fractures are not fully propped, even if they are stimulated. So, only the hydraulic fracture is explicitly discretized in the EDFM-MINC approach. The two sets of natural fractures are homogenized.

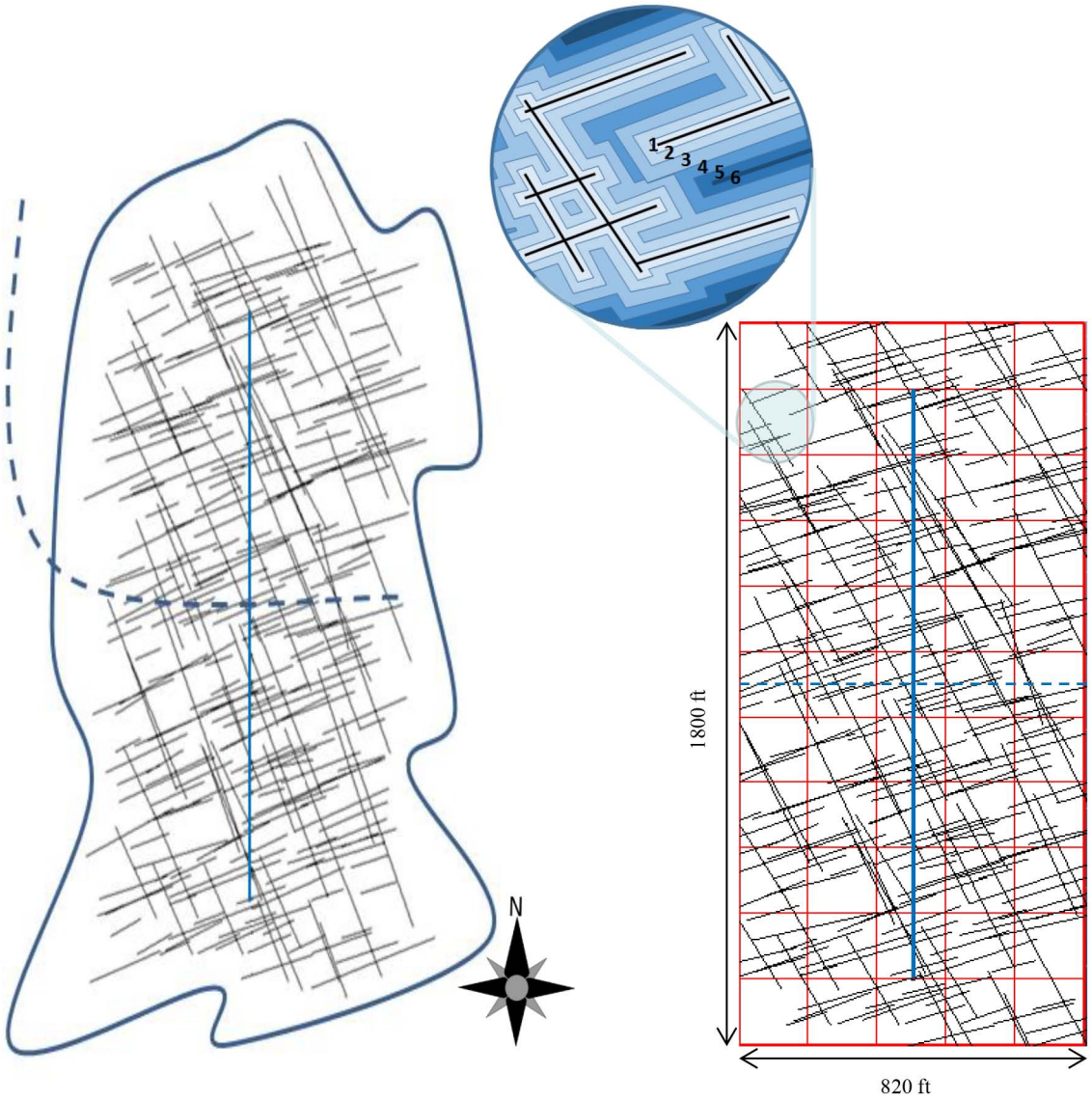

Figure 22—Stimulated fracture network around a hydraulic fracture in the synthetic case

In order to get a reference solution, very fine grid cells are used for the discretization of the matrix medium. All fractures are explicitly discretized. The flow exchange between a matrix cell and the fracture nodes is computed using the method described in Sarda et al. (2002). In the dual-porosity model and the EDFM-MINC approach, the reservoir domain is discretized by a 5 x 11 x 1 uniform grid (Fig. 22). Different upscaling methods for the computation of equivalent fracture permeability in the homogenized medium are compared for a single-phase flow simulation.

Single-phase flow simulation

First, we simulate a single-phase oil production problem. The matrix permeability is 0.0001 mD. Two fine grid simulations are performed with 2.2 million and 8.8 million matrix cells respectively, and compared in Fig. 23. These two simulations are very close, so we can consider them as the reference solution.

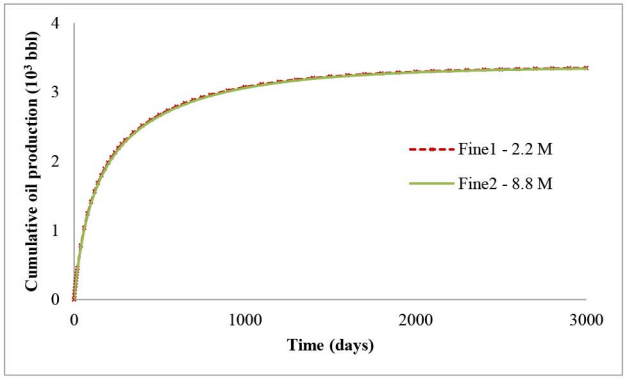

Figure 23—Single-phase fine grid simulations on the synthetic case

It is well known that homogenization of fractures is a big challenge, especially for the equivalent permeability calculation. This study allows us to check our proposed EDFM-MINC approach as well as different upscaling methods.

Three upscaling techniques are used to compute equivalent permeabilities, including an analytical method (Oda, 1986), a local numerical method at the scale of a grid cell, and a global upscaling method. For the local upscaling method, as only a few fractures are contained in a grid cell, the cell cannot be considered as a REV (Representative Elementary Volume). Hence, the error on equivalent permeabilities may be large. The global upscaling method consists of applying the numerical method by imposing the boundary condition on the whole SRV to get an estimation of the equivalent permeability. In this example, the global volume contains more than 250 connected fractures, and it can be considered as a representative elementary volume. Figure 24 compares the EDFM-MINC8 (a matrix cell is divided into 8 sub-cells) simulations using different equivalent permeabilities with the reference solution. As expected, the analytical method is not sufficiently accurate, and the local upscaling method is not accurate either, because the volume of a grid cell is too small to be representative. The global upscaling method, which is a numerical approach on a representative elementary volume, gives quite satisfactory result. Figure 24 presents also a dual-porosity simulation with the global upscaled permeability. This dual-porosity approach greatly underestimates the well performance and is not suitable for fractured low-permeability reservoir simulations.

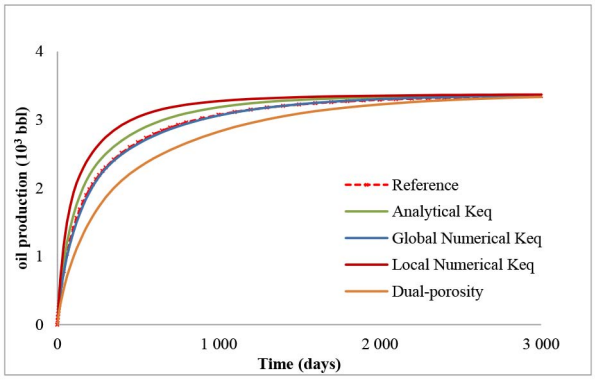

Figure 24—Comparison of different upscaling models for the single-phase flow simulation

In the following, the equivalent permeability obtained with the global upscaling method will be used for multiphase flow simulations.

Tight-oil with phase change

Now, let us simulate the multiphase tight-oil problem with a Black-oil model. The matrix permeability is 0.0001 mD. The initial reservoir pressure is 3800 psi, and the bottom-hole well flowing pressure is 1160 psi. The bubble point pressure is 2710 psi.

Initially, the reservoir is saturated with oil and mobile water. The rock is assumed to be water-wet. For the reference solution of this case, the matrix medium is discretized with 2.2 million cells. As shown by the previous test in a single matrix block, the use of a dual-porosity model is not appropriate to simulate flow phenomena related to phase changes, whereas the EDFM-MINC approach provides satisfactory solution thanks to the fine grid cells near the fracture faces. Such observations remain valid at the field scale as shown hereafter.

Figure 25 compares the oil and gas production for different simulations (EDFM-MINC, dual-porosity and the reference solution). Although some small differences are found among the EDFM-MINC methods, all the MINC simulations give reasonably accurate results compared to the reference solution, while the dual-porosity model greatly underestimate both the oil and gas productions. Figure 26 shows the evolution of GOR, which is similar for all simulations, including the dual-porosity simulation, during a very long period, of about seven years. In fact, the average homogenized fracture permeability is around 0.011 mD, and permeability contrast between the homogenized fracture medium and the matrix medium is not very high, around 100 times. Therefore, the fluid transferred from the matrix to the fracture cannot be immediately produced by the well. Then, the pressure inside the fracture remains high, especially in the regions far from the well, two-phase flow phenomena due to phase change inside the matrix is still limited in a small region. Therefore, the impact of matrix-fracture interaction on the phase change is not very significant. It has to be mentioned that our EDFM-MINC model does not take into account the exchange between a matrix cell and nearby fractures, and is not very accurate if several matrix blocks with very different sizes are contained in a simulation cell as discussed in the section below. So it is not a surprise that the EDFM-MINC is less accurate on this synthetic case than on a single-block presented above.

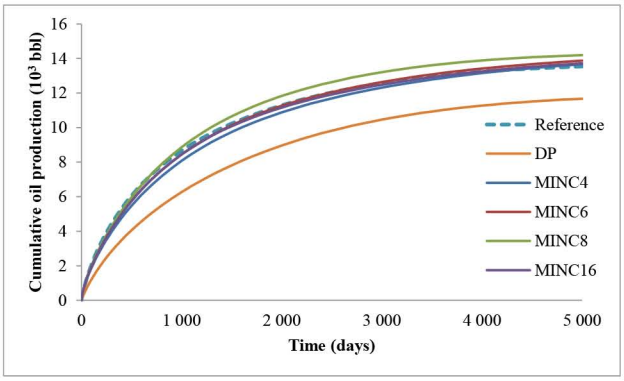

25a). Cumulative oil production

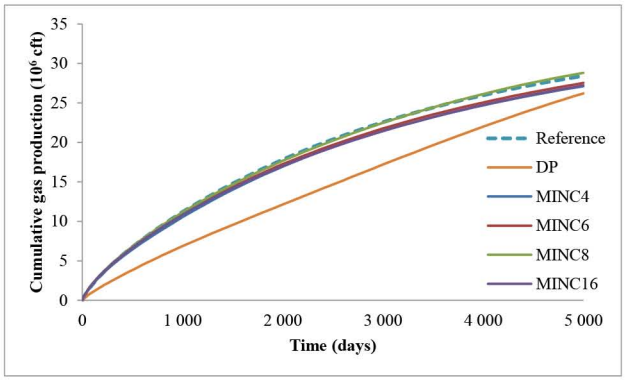

25b). Cumulative gas production

Figure 25—Tight-oil simulations in the synthetic reservoir with km = 0.0001 mD

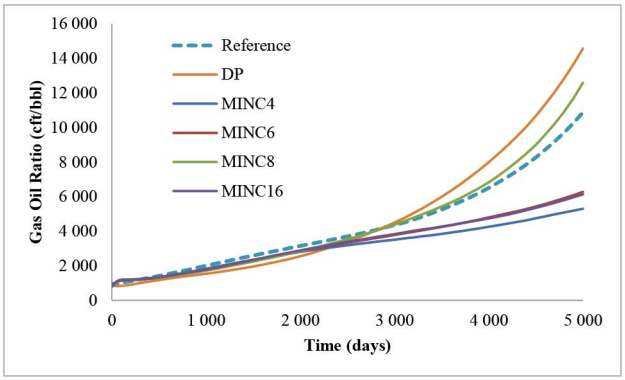

Figure 26—GOR for the tight-oil simulation with Km = 0.0001 mD

Figure 27 compares water production. At early times, the EDFM-MINC approach is close to the reference solution, thanks to their very fine grid cells near the fracture. But later, the EDFM-MINC approach fails to reproduce the reference solution, although it is still more predictive than the dual-porosity model. EDFM-MINC underestimates water production while the dual-porosity model largely overestimates it. For this case, water production is relatively low compared to the oil rate, due to the high capillary retention of the rock that is both tight and water-wet.

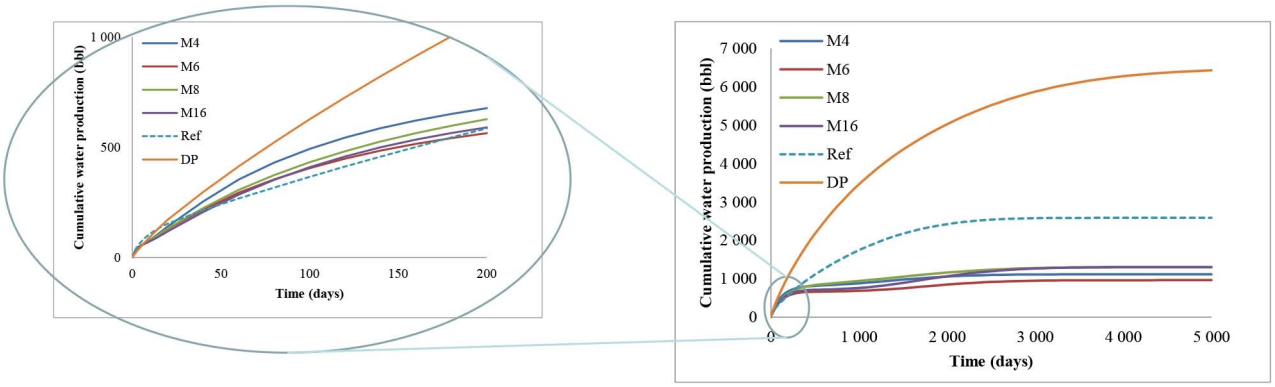

Figure 27—Cumulative water production with Km = 0.0001 mD

Now, we increase the fracture matrix permeability contrast and consider a matrix permeability of 0.00001 mD. Figure 28 presents the oil and gas daily rate for this case. Again, all MINC simulations are accurate enough. The dual-porosity model greatly underestimates the oil rate during the first 2 years, and overestimates it later on. For the gas production, the dual-porosity model underestimates it for more than 10 years. Figure 29 shows the GOR. In this test, the EDFM-MINC method simulates correctly the pressure drop and the phase change near the fractures, while the dual-porosity model delays the phase change behavior in the near-fracture zone due to higher matrix pressure. Figure 30 presents the cumulative water production. In this extremely low permeability case, the water production is satisfactorily simulated with the EDFM-MINC method.

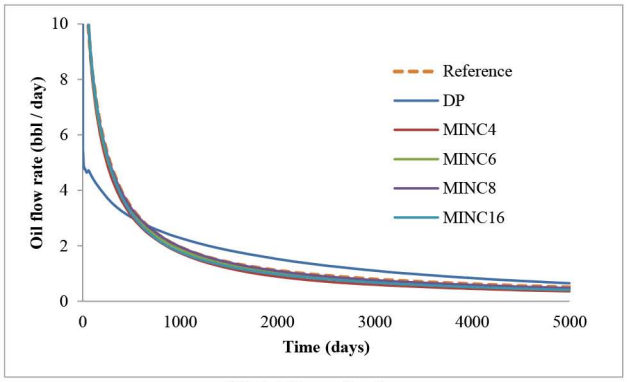

28a). Oil production

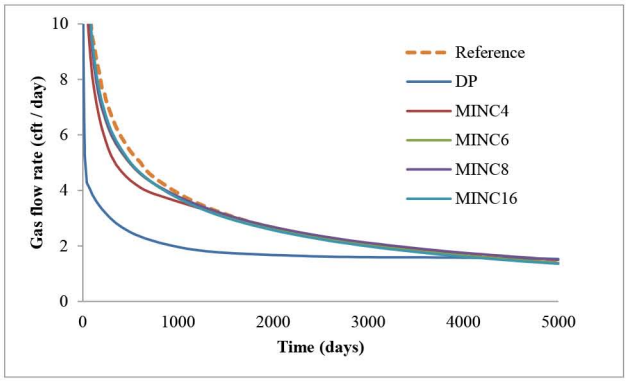

28b). Gas production

Figure 28—Tight-oil simulations with Km = 0.00001 mD

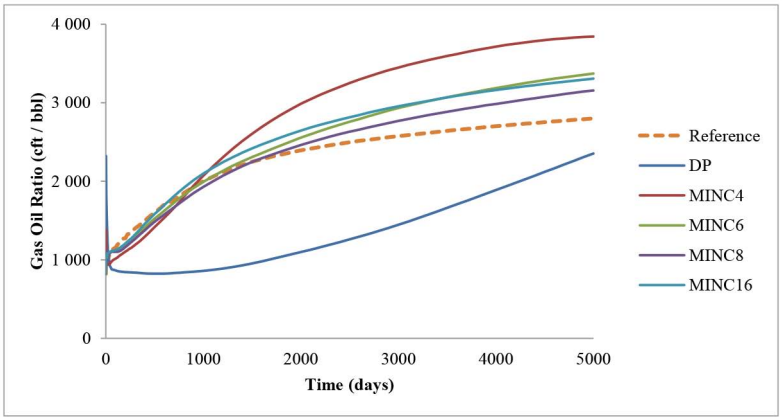

Figure 29—GOR in the synthetic reservoir with Km = 0.00001 mD

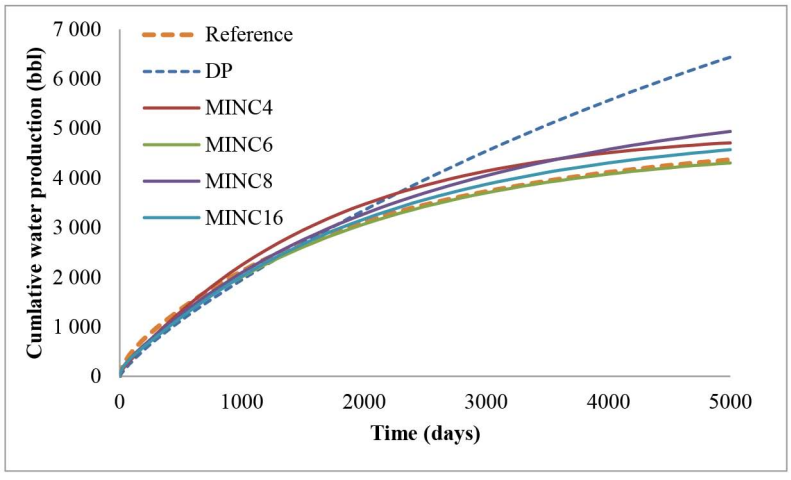

Figure 30—Cumulative water production in the synthetic reservoir with Km = 0.00001 mD

Shale-gas with condensate

We consider a liquid-rich gas-condensate reservoir with a retrograde condensation issue. The gas composition is the same as in the single matrix block case presented above (**Table 2**). The initial reservoir pressure is 6000 psi, and the bottom-hole well pressure is 1200 psi. The dew point pressure is around 3000 psi. For this gas-condensate case, we encountered a numerical convergence issue for the fine-grid simulation with 2.2 million matrix cells. That issue could not be investigated for lack of time, hence the reference solution was obtained on a coarser model, with 550000 matrix cells.

Figure 31 compares gas and condensate productions simulated with various EDFM-MINC models, the dual-porosity approach and the reference solution. All MINC simulations are close to the reference solution. The dual-porosity model is not accurate, especially for the condensate simulation. Figure 32 shows the produced condensate-gas ratio from the well. The initial value of 0.00004 bbl/cft corresponds to the condensate content of the reservoir fluid in its initial single-phase state. At very early times, the produced condensate-gas ratio starts to decrease, because the pressure drops below the dew point pressure in the outer parts of matrix blocks near fractures, thus causing a condensate deposit that is preferentially retained there while reducing gas production from the matrix medium. This phenomenon is reproduced by the fine-grid simulation model (reference solution) and using the MINC method. However, when using a dual-porosity model, the condensate-gas ratio remains constant for more than one year, because the pressure in the matrix cells remains higher than the dew point pressure during that initial period of production.

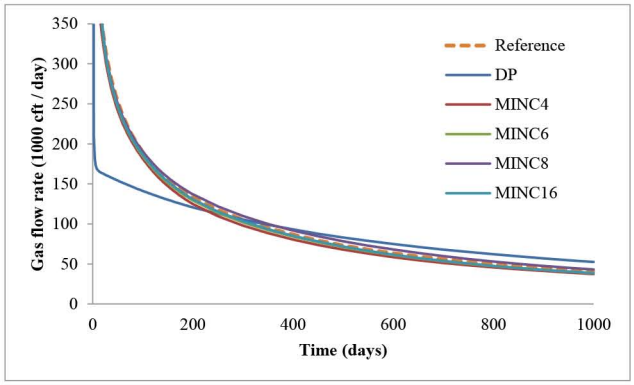

31a). Gas production rate

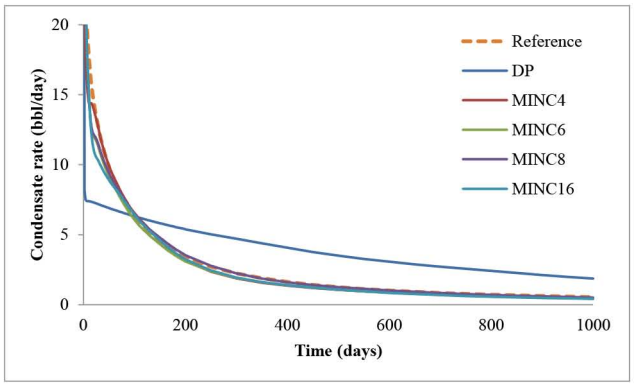

31b). Condensate production

Figure 31—Gas condensate reservoir in the synthetic case with Km = 0.00001 mD

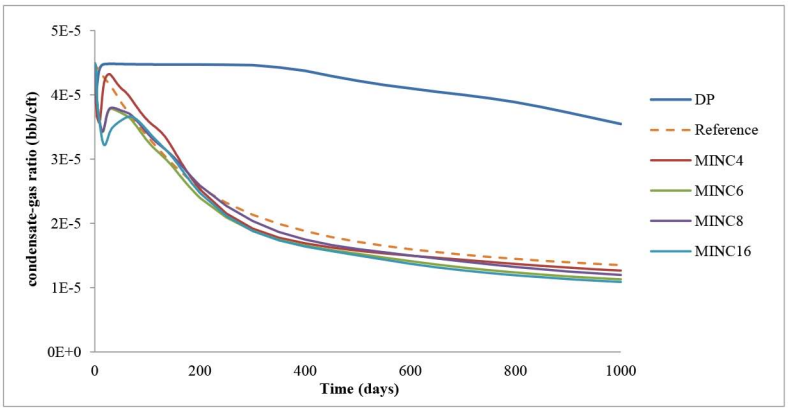

Figure 32—Condensate-gas ratio in the gas synthetic case

From the simulation results, we also notice that although all MINC subdivisions give globally satisfactory results, increasing the number of matrix subdivisions does not always ameliorate again the accuracy. In fact, with complex physics, such as a multi-phase flow with phase change, the simulation results, especially GOR, are very sensible to the grid sizes near the fractures. Nevertheless, we notice that the general trends are good.

Table 3 summarizes the CPU times for the EDFM-MINC and the fine grid single-porosity simulations. Using the EDFM-MINC model, the CPU time is reduced from several hours to less than one minute.

Table 3—CPU time comparison

Case	Explicit Discretized Model (Single-porosity)		Discrete Fracture Model (MINC8)	
	Number of grid cells	CPU Time	Number of grid Cells	CPU Time
Single-phase flow	2 200 624	5 hrs.	504	20 secs
Tight-oil three phase flow		7 hrs.		30 secs.
Retrograde gas	550 624	30 hrs		37 secs.

In summary, the EDFM-MINC method is successfully applied to the synthetic case, where two families of fractures are generated using a geostatistical model. In general, the MINC approach gives quite satisfactory results for both tight-oil and shale-gas simulations, because of its ability to handle the phase change impact on matrix-fracture interaction. The gain in CPU time is significant. Although this method is not always as accurate as the reference solution depending on the MINC subdivisions, the obtained results are much better than those from a dual-porosity simulation. On the other hand, the conventional dual-porosity model is not suitable for low-permeability reservoir simulations, while the EDFM-MINC approach improves greatly the accuracy. The EDFM-MINC provides a good compromise between simulation accuracy and efficiency in computational time.

Discussions and Further Improvements

It is well known that a standard dual-porosity model cannot simulate correctly the matrix-fracture exchange because matrix blocks are not sub-gridded and because a single average block size is considered in dual-porosity cells containing several matrix blocks of different sizes. Previous simulation examples have shown that the MINC method can overcome the former limitation. The present section aims at demonstrating that the MINC method may also be a solution to take into account the non-uniform distribution of matrix block sizes at reservoir simulation cell scale.

Modelling the matrix-fracture interaction for blocks of various sizes requires accounting for the fact that small blocks contributes only to the early stage of production, while large blocks contribute to both early and late stages. Regarding the EDFM-MINC model, the transmissibility formula given by Eq. (13) for the inter-porosity flow calculation needs to be corrected. Otherwise, the matrix-fracture exchange rate will be overestimated, because the fluid in an inner subdivision of a large matrix block is driven to the fracture through larger exchange surfaces, which are the sum of the exchange surfaces of all the matrix blocks in the considered cell.

Figure 33 shows an example of a simulation cell with size 300 ft by 300 ft surrounded by fractures and containing also two orthogonal fractures inside. This cell is composed of 4 rectangular matrix blocks with sizes of 30 ft x 30 ft for the block B_1, 30 ft x 270 ft for the block B_2, 270 ft x 30 ft for the block B_3, and 270 ft x 270 ft for the block B_4. The fracture aperture and permeability are set at 0.004 ft and 2500 mD respectively, and the matrix permeability is 0.0001 mD. A single-phase gas flow simulation is performed. Figure 34 presents a comparison of the MINC6 approach and the reference solution obtained with very fine grid cells. We observe that the MINC method is only accurate during the first 150 days, and that it overestimates the gas production afterwards. The increasing inaccuracy of MINC method at late times is related to the different sizes of the matrix blocks contained in the cell.

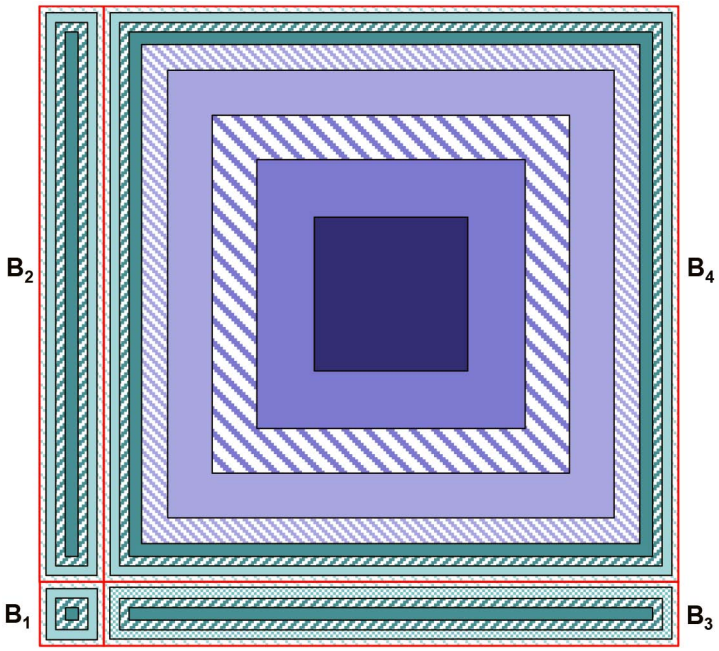

Figure 33—MINC subdivision in a simulation cell containing four matrix blocks with different sizes

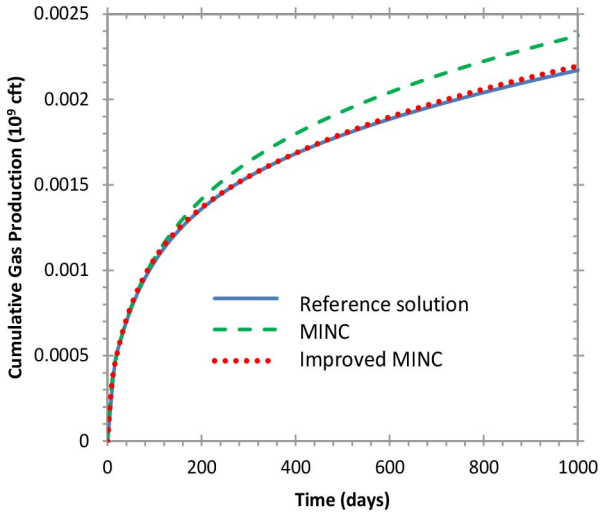

Figure 34—Simulation results in a cell containing matrix blocks of different sizes

To illustrate the origin of this inaccuracy, Figure 35 plots the cumulative matrix volume versus the distance from the fractures in each of the four matrix blocks as well as the total cumulative volume versus the distance from fractures in the simulation cell (blue curve). This type of curve is the basis for calculating the matrix-fracture transmissivity in the MINC model, as formulated by Eqs. 13 and 14. Clearly, the maximum distance found in Block B_1 is the same as that in B_2 and B_3, and the curves for B_2 and B_3 are the same. However, the maximum distance of exchange is much larger for Block B_4 that is a large square block. For this reason, the matrix-fracture flow transfer is completed after a much longer time for that matrix block than for the other blocks. It has to be mentioned that the flow exchange between a matrix block and the fractures is limited in that matrix block. In other words, the exchange surface for the fluid in a block B_i should be calculated using the cumulative curve of the block B_i. However, the MINC transmissibilities determined from Eq.(13) are based on the total cumulative distribution curve, which corresponds to the sum of all the curves for small distance from the fractures and to the curve from B_4 alone for large distances. Therefore, when the fluid from the center of B_4 is produced into the fractures, the exchange surface area is

overestimated in the near fracture zone due to the contribution from the small blocks in that surface area. This leads to an overestimation of the gas production at late times.

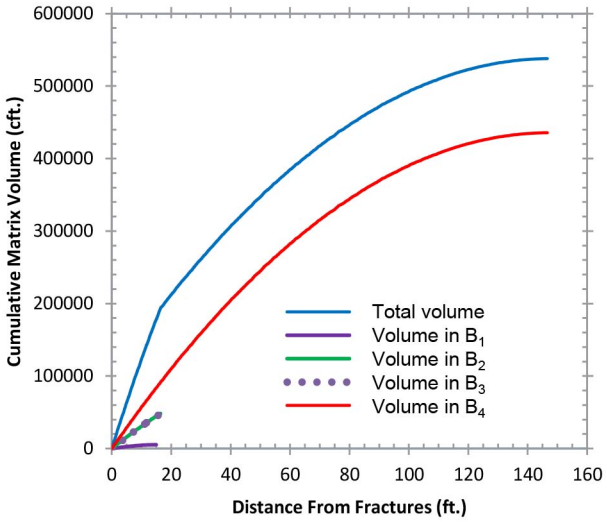

Figure 35—Cumulative volume versus distance for blocks of different sizes

To overcome this inaccuracy, we suggest modifying the transmissibility values when the contribution of a matrix sub-block ends in the total cumulative distribution curve, to take into account only the producing blocks. In the example illustrated by Fig. 33, the exchange surface is calculated with all the four sub-blocks when the distance is smaller than 15 ft, but has to be computed with the sole Block B_4 when the distance is larger than 15 ft. To that end, the transmissibility $T_{i,i+1}$ between MINC subdivisions i and $i+1$ such that $d_i \leq 15 < d_{i+1}$ is corrected by the additional term $T'_{i,i+1}$ so that the flow from the subdivision #(i+1) to the fracture under a steady-state regime corresponds to the transfer from Block B_4 alone, that is,

$$\frac{1}{T'_{i,i+1}} + \sum_{j=0}^{i-1} \frac{1}{T_{j,j+1}} = \sum_{j=0}^{i} \frac{1}{T^4_{j,j+1}} \tag{17}$$

where $T_{j,j+1}$ $(j = 0, 1, \ldots i\text{-}1)$ is the transmissibility calculated by Eq. (13) using the total cumulative distribution function, $T^4_{j,j+1}$ and is the transmissibility calculated with the cumulative distribution of only Block B_4.

Figure 34 presents also the simulation with the MINC6 approach using the modified transmissibility. With the corrected transmissibility, the result is greatly improved.

We have shown that it is possible to use an appropriate MINC approach to handle the matrix-fracture interaction for a simple distribution of blocks of different sizes. How to handle this issue of matrix-fracture interaction with various block sizes in the context of the DFN is our ongoing work.

Conclusions

Unconventional shale-gas or tight-oil reservoirs are characterized by multi-scale fractures of various sizes embedded in extremely low-permeability formations, which increases the complexity of the reservoir simulation. A single-porosity model with explicitly discretized fractures is accurate for flow simulation, but it takes too much CPU time and is almost unfeasible for field applications. A standard dual-porosity model is not accurate, because of the extremely-long transient period in matrix-fracture interaction due to the ultra-low permeability of the matrix medium and to the non-linear evolution of pressure inside the matrix blocks.

To handle multi-scale fracture networks, one solution is the EDFM approach, but it is still necessary to correctly treat the interactions between different media.

In this paper, we present an EDFM-MINC approach to simulate shale reservoirs. We also propose several techniques to ameliorate transmissibility computations for flow exchanges between the various media of an EDFM. Fractures are classified according to their conductivities. Hydraulic and propped fractures are explicitly discretized, and all other fractures, including stimulated and non-stimulated natural fractures, are homogenized. For matrix and fracture interaction, a MINC proximity function is used to subdivide the matrix medium to treat the matrix-fracture flow exchange in a fully transient way. In this EDFM-MINC approach, equivalent permeability and porosity values are determined for the low-conductivity fractures only, while the matrix-fracture exchange involves all sorts of fractures with the MINC modeling method. Moreover, the transmissibility computation between the explicitly discretized fracture and the homogenized medium can be improved by taking into account the pressure distribution via an integral method. A transmissibility formula between SRV and non-SRV zones associated to the MINC method is also derived.

The proposed EDFM-MINC approach is tested on both single-phase and multi-phase flow with phase change in the presence of discrete fracture networks. This method provides quite satisfactory results, compared to the fine-grid single-porosity simulation with an explicit discretization of fractures. It can be used to simulate tight-oil reservoirs as well as gas-condensate ones. Moreover, this method reduces significantly the number of grid cells, leading to decrease in the CPU time, compared to the single-porosity model. The EDFM-MINC offers a computationally efficient approach for simulating fluid flow in fractured low-permeability reservoirs, and provides a compromised solution between simulation accuracy and CPU time.

This promising EDFM-MINC approach calls for further developments to take into account the distribution of matrix blocks at the scale of reservoir cells. How to efficiently handle this kind of problem is our ongoing work.

Acknowledgement

The authors gratefully acknowledge IFP Energies nouvelles for their support.

Nomenclature

a = *matrix block dimension*
A = *exchange area*
b = *matrix block dimension*
C = *mole fraction*
d = *distance*
F = *flux*
g = *gravitational acceleration*
J = *diffusion/dispersion term*
k = *absolute permeability*
k_r = *relative permeability*
P = *pressure*
Q_{kj} = *flow rate between cell k and fracture node j*
Q^{mf} = *matrix-fracture exchange term*
q = *source/sink term*
S = *fluid saturation*
t = *time*
T = *transmissibility*

$\vec{u}$ = *velocity*
v_{sg} = *gas sorption term*
V = *volume*
Z = *depth*
φ = *effective porosity of formation*
Φ = *flow potential*
λ_p = *mobility of phase p*
ζ = *cumulative fraquency*
ρ = *mole density*
μ = *viscosity*
σ = *shape factor*

Superscript

f = *fracture*
F = *high conductivity fracture*
m = *matrix*
M = *m or f*

Subscript

c = *component*
f = *fracture*
g = *gas*
i = *cell index*
j = *cell or node index*
k = *cell index*
m = *matrix*
o = *oil*
p = *phase*
w = *water*

References

Cai, L., Ding, D. Y., Wang, C., and Wu Y-S. (2015) "Accurate and Efficient Simulation of Fracture–Matrix Interaction in Shale Gas Reservoirs" *Transport in Porous Media*, vol. **107**, issue 2, Match, pp305-320.

Delorme, M., Daniel, J. M., Kada-Kloucha, C., Khvoenkova, N., Schueller, S., and Souque, C. (2013) "An Efficient Model to Simulate Reservoir Stimulation and Induced Microseismic Events on 3D Discrete Fracture Network for Unconventional Reservoirs", SPE 168726, presented at Unconventional Resources Technology Conference, Denver, CO, USA, August.

Ding, D. Y., Wu, Y. S., Farah, N., Wang, C. and Bourbiaux, B. (2014) "Numerical Simulation of Low Permeability Unconventional Gas Reservoirs", SPE 167711, presented at the SPE/EAGE European Unconventional Ressources Conference and Exhibition, Vienna, Austria, 25-27 Feb.

Ding, D. Y., Wu, Y-S. and Jeannin, L. (2014) "Efficient Simulation of Hydraulic Fractured Wells in Unconventional Reservoirs" *J. of Pet. Sci. & Eng.*, vol. **122**, Oct. pp631-642.

Famy, C., Bourbiaux, B. and Quintard, M. (2005) "Accurate Modelling of Matrix-Fracture Transfers in Dual-Porosity Models: Optimal Sub-Gridding of Matrix Blocks, SPE paper No. 93115 presented at the SPE Reservoir Simulation Symposium, Houston, 31 Jan.-2 Feb.

Farah, N., Ding, D. Y. and Wu, Y. S. (2015) "Simulation of the Impact of Fracturing Fluid Induced Formation Damage in Shale Gas Reservoirs", SPE 173264, presented at the SPE Reservoir Simulation Symposium, Houston, Texas, 23-25 Feb.

Farah, N. and Ding, D. Y. (2016) "Discrete Fracture Model based on Multiple Interacting Continua Proximity Function for Unconventional Low Permeability Reservoir Simulations" proceeding of 15th ECMOR, Amsterdam, Netherlands, 29 August - 1 Sept.

Farhadinia, M. A. and Delshad, M. (2010) "Modeling and Assessment of Wettability Alteration Processes in Fractured Carbonates Using Dual Porosity and Discrete Fracture Approaches" SPE 129749 presented at the SPE Improved Oil Reco., Tulsa, OK, USA, 24-28 April.

Hajibeygi, H., Karvounis, D., and Jenny, P. (2011) "A hierarchical fracture model for the iterative multi-scale finite volume method", *Journal of Computational Physics*, Vol. **230**, pp8729–8743.

Jiang, J., Shao, Y. and Younis, R. M. (2014) "Development of a Mumti-Continuum Multi-Component Model for Enhanced Gas Recovery and CO2 Storage in Fractured Shale Gas Reservoirs" SPE 169114, presented at the SPE Improved Oil Rec. Symp., Tulsa, USA, 12-16 April.

Jiang, J. and Youis, R. M. (2016) "Hybrid Coupled Discrete-Fracture/Matrix and Multicontinuum Models for Unconventional-Reservoir Simulation" *SPE Journal*, June, pp1009-1027.

Karimi-fard, M., Durlofsky, L. J., and Aziz, K. (2004) *"An efficient discrete-fracture model applicable for general purpose reservoir simulators", SPE Journal*, Vol. **9**, pp227–236.

Khvoenkova, N., & Delorme, M. (2011). An optimal method to model transient flows in 3D discrete fracture network. In IAMG conference.

Khvoenkova, N., Bossie-Codreanu, D, Broussard, N., Delorme, M. and Lecomte, JC. (2015) "Application of the DDFN (Discrete and Deformable Fracture Network) Method within an Integrated Unconventional Reservoir Study Workflow", SPE 175112 presented at the SPE ATC&E Houston, Texas, USA, 28-30 September.

Lee, S. H., Lough, M. F., and Jensen, C. L. (2001) "Hierarchical modelling of flow in naturally fractured formations with multiple length scale", *Water Resources Research*, **37** (3), December, pp. 443-445.

Li, L. and Lee, S. H. (2008) "Efficient Field-Scale Simulation of Black Oil in a Naturally Fractured Reservoir Through Discrete Fracture Networks and Homogenized Media", *SPEREE J.* August, pp750-758.

Matthai, S., Menzentsev, A. and Belayneh, M. (2005) "Control-Volume Finite-Element Two Phase Flow Experiments with Fractured Rock Represented by Unstructured 3D Hybrid Meshes", SPE 93341, SPE Reservoir Simulation Symposium, Houston, USA, Fab.

Mirzaei and Cipolla C. L. (2012) "A Workflow for Modelling and Simulation of Hydraulic fractures in Unconventional Gas Reservoirs", paper SPE 153022, Middle East Unconventional Gas Conference and Exhibition held in Abu Dhabi, UAE, January 23-25.

Moinfar, A., Narr, W., Hui, M. H., Mallison, B., and Lee, S. H. (2011) "Comparison of Discrete-Fracture and Dual Permeability Models for Multiphase Flow in Naturally Fractured Reservoirs", paper SPE 142295, Reservoir Simulation Symposium held in The Woodlands, Texas, USA, 21-23, Feb.

Moinfar, A., Varavei, A., Sepehnoori, K., and Johns, R. T. (2013) "Development of a coupled Dual Continuum and Discrete Fracture Model for the Similation of Unconventional Reservoirs", paper SPE 163647, Reservoir Simulation Symposium held in The Woodlands, Texas, USA, February 18-20.

Norbeck, J., Huang, H., Podgorney, R., and Horne, R. (2014) "An Integrate Discrete Fracture Model for Description of Dynamic Behavior in Fractured Reservoirs", Departement of Energy Resources Engineering, Stanford University, California, USA, February 24-26.

Oda, M. (1986) "Permeability Tensor for Discontinuous Rock Masses", *Geotechnique Volume* **35**, pp483–495.

Pruess, K. and Narasimhan, T. N. (1985) "A Practical Method for Modeling Fluid and Heat Flow in Fractured Porous Media", *Society of Petroleum Engineers Journal*, paper SPE 10509, Reservoir Simulation Symposium held in New Orleans, January 31 - February 3.

Sarda, S., Jeannin, L., Basquet, R. and Bourbiaux, B. (2002) "Hydraulic Characterization of Fractured Reservoirs: Simulation on Discrete Fracture Models", *SPEREE*, pp154-162, April.

Sun, J. and Schechter, D. (2015) "Optimization-Based Unstructured Meshing Algorithms for Simulation of Hydraulically and Naturally Fractured Reservoirs with Variable Distribution of Fracture Aperture, Spacing, Length and Strike", *SPE Reservoir Evaluation & Engineering* **18** (04), pp463–480.

Xu, Y., Cavalcante Filho, J. S. A., Yu, W. and Sepehrnoori, K. (2016) "Discrete-Fracture Modeling of Complex Hydraulic-Fracture Geometries in Reservoir Simulators" *SPEREE*, August, pp1-20.

Wu, Y. S. and Pruess, K. (1988) "A Multiple-Porosity Method for Simulation of Naturally Fractured Petroleum Reservoirs", *SPE Reservoir Engineering*, **3**, pp327–336.

Wu, Y. S., Li, J., Ding, D., Wang, C. and Di, Y. (2014) "A Generalized Framework Model for Simulation of Gas Production in Unconventional Gas Reservoirs" *SPE Journal*, vol. **19**, issue 5, pp845-857.